1-1-1999

Efficacy of Beam-Hardening Correction for Vascular Morphometry Using 3D Conebeam Micro-CT

Roger H. Johnson
Marquette University

Jiang Hsieh
GE Medical Systems

Robert C. Molthen
Marquette University, robert.molthen@marquette.edu

Christopher A. Dawson
Medical College of Wisconsin

Efficacy of Beam-hardening Correction
for Vascular Morphometry Using 3D Conebeam Micro-CT

[1,3,4,6]Roger H. Johnson, [2]Jiang Hsieh, [1,6]Robert C. Molthen and [1,5,6]Christopher A. Dawson

[1]Department of Biomedical Engineering, Marquette University
[2]Applied Science Laboratory, GE Medical Systems,
Departments of [3]Radiology, [4]Biophysics and [5]Physiology, Medical College of Wisconsin
[6]Research Service, Zablocki VA Medical Center, Milwaukee, Wisconsin, USA

INTRODUCTION:

Basic CT theory is based on the assumption of monochromaticity of the x-ray beam[1]. Since the x-ray spectra emitted by electron-impact tubes are polychromatic, artifacts can arise in the reconstruction which may pose problems for quantitative morphometric and physical density measurements. We report our initial application of an iterative approach for beam-hardening correction to volumetric micro-CT images of contrast-enhanced, excised rodent lungs and contrast agent-mimicking wire phantoms.

MATERIALS AND METHODS:

Micro-CT Data Acquisition:

Our scanner, shown in Figure 1, consists of a microfocal x-ray source, specimen manipulator and image intensifier (II) detector coupled to a CCD camera. The 5- to 100-kVp, 10- to 300-microamp x-ray source produces spots as small as 3 μm in diameter. The xyzΘ stage translates and rotates the specimen. The II has spatial resolution of 5.3, 6.2 and 7.2 lp/mm in the 9-, 7- and 5-inch modes. The CCD camera has recently been upgraded from a Sony XC-75 with 640 by 480-pixel matrix (interline transfer) read out with the NTSC standard (8 bits, interlaced, 30 fps) to a Silicon Mountain Design SMD1M-15 with 1024^2-pixel matrix (frame transfer) read out at selectable rates with 12-bit dynamic range. A number of acquired frames were averaged before digitizing with an Imaging Technology ITI IM-PCI frame grabber.

For our initial studies of vascular morphology, we acquired images of contrast-enhanced mouse, rat and dog vascular beds. The bronchus and pulmonary artery or the coronary artery were cannulated before excising the organ and the vessels flushed clear of blood. A brominated perfluorocarbon (barium-gelatin mixture) contrast agent was then introduced into the pulmonary (coronary) arterial tree. During imaging, the contrast agent and airway pressures were held constant. To provide a gold standard for future studies of diameter measurement accuracy, we imaged a phantom containing 1.0-, 0.5-, 0.2-, 0.1- and 0.05-mm Ti6Al4V alloy wires which exhibit x-ray attenuation characteristics almost identical to those of the brominated perfluorocarbon (Perflubron®), as calculated by the rule of mixtures[2]. Three hundred sixty views were acquired over a full rotation of the specimen, using (half) cone angles of $<7°$. The remaining important parameters for data acquisition are given in Table 1.

Image Reconstruction and Data Processing:

Projection preprocessing[3] included centering the rotation axis; correcting the geometric distortion of the II by polynomial unwarping using coefficients determined by use of a ball-bearing (BB) phantom[4]; and dividing by a flood field to correct for the non-uniform illumination. The data were reconstructed using the Feldkamp conebeam reconstruction algorithm[5] on an isotropic grid of dimension given in Table 1. Measurements of vessel segment length and diameter and branching angles are made either from arbitrarily-oriented

image planes or from the volumetric data. Data exploration is facilitated by surface-shaded renderings of thresholded, binary data produced using IDL® software.

To decrease measurement and segmentation errors caused by polychromatic streak and other artifacts, we have begun investigating pre- and postprocessing methods to correct for non-uniform and non-linear detector element response and for beam hardening. We have applied an iterative beam-hardening correction in image space, using a tilted, parallel beam reprojection-backprojection technique as described in reference[6]. The efficacy of the correction method was evaluated qualitatively by examination of line scans across artifact-affected vessel diameters and of difference images between before- and after-correction image sets.
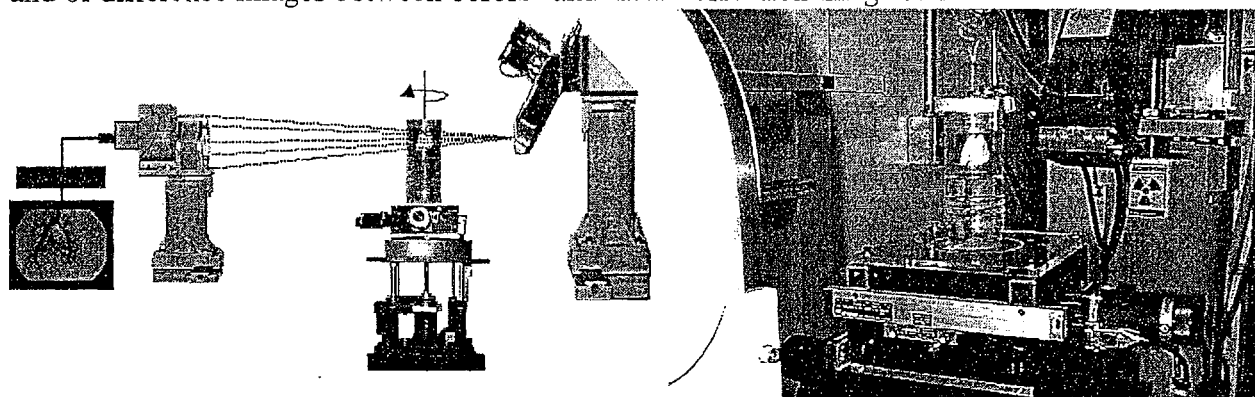

Figure 1: Scanner with a rat lung in place for imaging. The source is on the right, specimen in the middle and detector on the left.

Table 1: Data acquisition and reconstruction parameters

Parameter	Rat Lung	Dog Heart	Wire Phantom	Mouse Lung
kVp	49	66	32, 49	32, 43, 98
tube current (milliamps)	49	64	32, 49	32, 44, 25
source-to-detector (cm)	70.0	143.8	68.1	53.3
source-to-center (cm)	20.0	60.0	18.0	7.5
II mode	7-inch	9-inch	7-inch	5-inch
frames per view	7	7	10	10
acquisition matrix (pixels)	480^2	480^2	512^2	512^2
reconstruction matrix	457^3	449^3	497^3	497^3
reconstruction volume (cm^3)	3.5	9.6	3.5	1.6

RESULTS:

To illustrate the complex structure of the vascular trees we want to quantify morphometrically, Figure 2 shows renderings of the vascular beds of lungs and heart from rodents and dog. Figure 3 shows transverse slices through the proximal rat lung before and after application of the beam hardening correction. The line scans shown across the two lobar arteries are plotted for both cases below the images. Figure 4a shows an as-reconstructed transaxial wire phantom image acquired at 32 kVp, and 4b shows the same image after beam hardening correction. Figure 4c shows the line scan plots illustrated on the figure (thin line: as reconstructed; thick: corrected), while 4d shows identical line scans from an image (not shown) acquired at 49 kVp. Figure 5a depicts the as-reconstructed 32-kVp wire phantom image, indicating the location of the line scans plotted in Figure 5b. The upper, heavier plot corresponds to the more-nearly vertical line; the lower to the horizontal line through the beam hardening-affected regions.
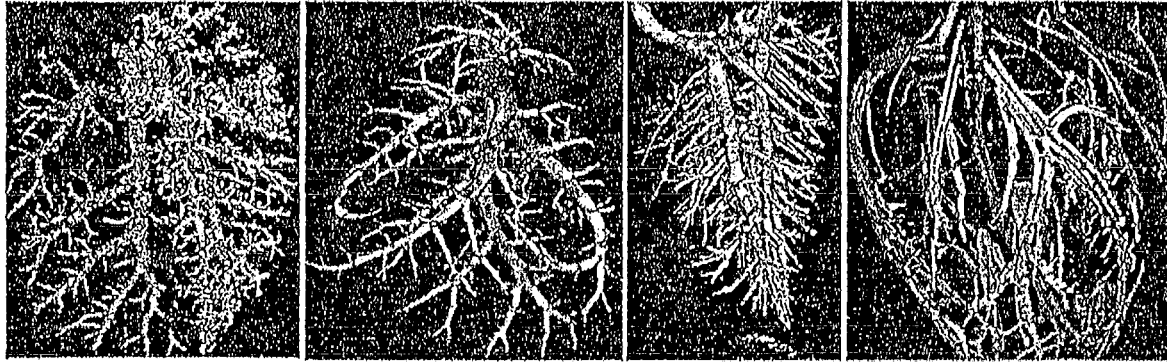
Figure 2: Surface-shaded renderings of the mouse, rat and dog lung and the dog heart. In the rodent lungs, only the arterial tree is filled with contrast, whereas both arterial and venous trees are visualized in the dog lung and heart.
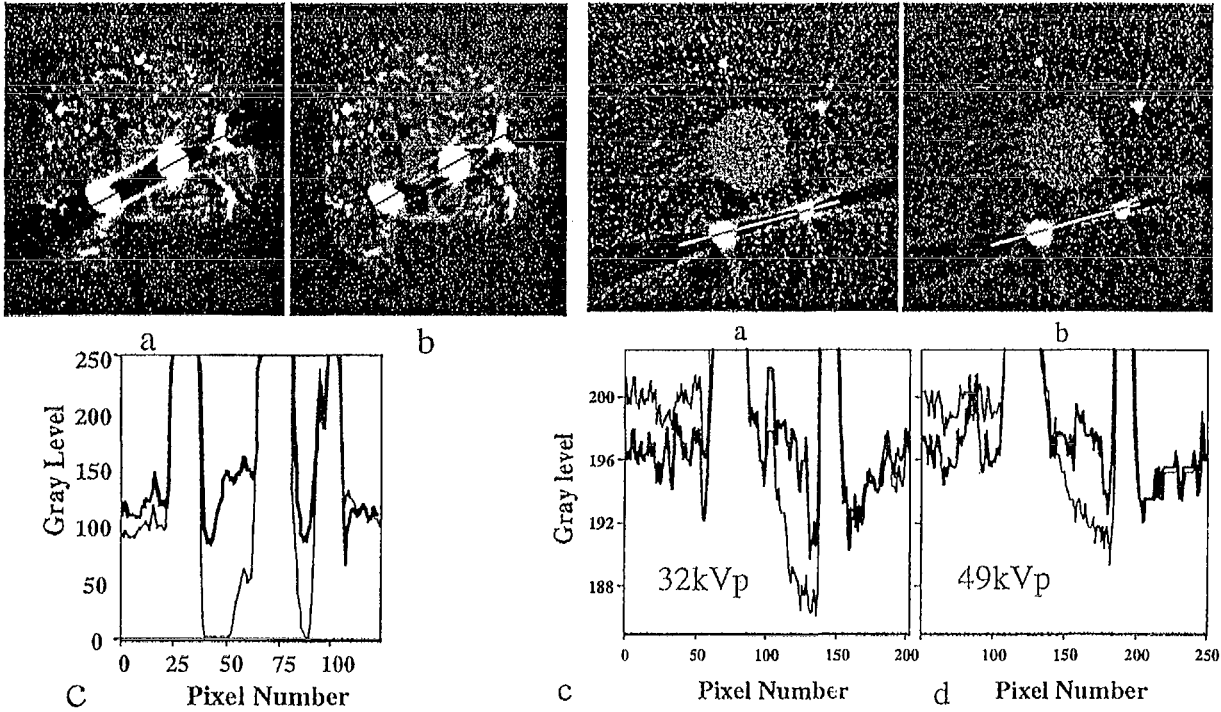

Figure 3: a) as-reconstructed and b) corrected image of proximal rat lung. Plot of indicated line scans. Lower line ⇔ as-reconstructed image.

Figure 4: a) as-reconstructed and b) corrected 32-kVp image of wire phantom and c) plot of indicated line scans. d) Plot of identical line scans, but from 49-kVp data set.
Thin line ⇔ as-reconstructed image data.

Figure 5: Uncorrected transaxial slice through Ti-alloy wire phantom showing beam hardening and location of linescans plotted to the right. Upper, bold plot corresponds to nearly-vertical line and shows "true" background gray level.
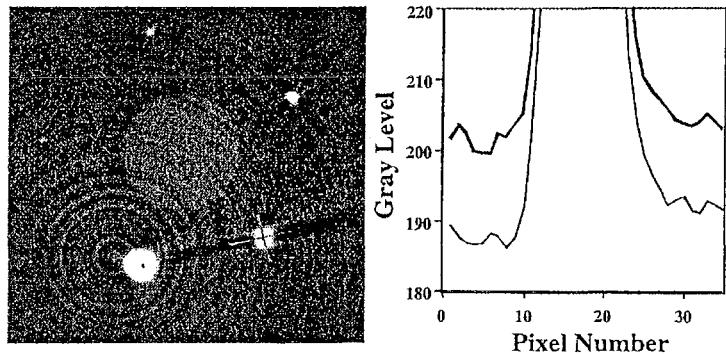
DISCUSSION AND CONCLUSION:

With polychromatic illumination, the beam spectrum changes as it passes through various materials in the sample, causing the attenuation at a point in the object volume to depend on the direction of the ray (beam) passing through the point[1]. This causes the well-known beam-hardening artifacts, since the center of dense objects are "seen" by a higher-energy beam making them appear less dense than they are and causing cupping artifacts in the reconstruction. The inconsistency in the data set due to the differences in detected spectra in the specimen vs. the reference (flood) projections also give rise to streak artifacts, which tend to connect high-density objects, like contrast-enhanced vessels, in the reconstructed images. If not minimized, these streaks can contain large negative numbers in the reconstruction which are not only physically unrealistic, but can cause errors in extracted metrics, particularly vessel lumen diameters, and pose problems for segmentation routines. The causes of artifacts can be constrained by exploiting the relevant physics, for example using energy-sensitive detectors, mono- or quasimonochromatic illumination[7], prehardening the beam[8], or calibrating detector elements' responses using well-characterized materials of various thicknesses[9]. But these approaches all have limitations for laboratory micro-CT: most detectors are energy-integrating, the sources are Bremsstrahlung, low-energy photons improve soft-tissue contrast, material-specific calibration fails for multi-constituent specimens, and individual detector calibration is burdensome for conebeam CT, since many thousands of elements are used[10].

Alternatively, artifacts may be reduced by projection processing or post-processing of the reconstruction, as we have attempted here. Our results show the early promise of this approach: The soft tissue (airway) detail between the highly-attenuating vessels in Figure 3 is evidently improved by the correction method, and the artifactually-low densities in that region have been raised, as evidenced by the line-scan plot, closer to the "true" level of parenchymal regions remote from vessels. The same effect is confirmed by Figure 5. Figure 4 verifies the conventional wisdom that higher kVp decreases beam-hardening effects, and again shows the ability of the proposed method to improve the accuracy of the background reconstruction between wires, actually lowering the background density to the left of the 1-mm wire, while raising it between the thick wires. We intend to continue this line of study in order to move from the merely qualitative image information we show here to produce semi-quantitative density information using micro-CT. Dispensing with the image intensifier and implementing calibration protocols similar to those applied to advantage in clinical CT will be essential steps in this progression.

REFERENCES:

1) Herman, GT, Image Reconstruction from Projections: The Fundamentals of Computerized Tomography, Academic, New York, 1980.

2) White, DR, Med. Phys. 5(6):467-79, 1978.

3) Johnson, RH, Hu, H, Haworth, ST, Cho, PS, et al., Phys. Med. Biol. 43(4):929-40, 1998.

4) Cho, PS and Johnson, RH, Phys. Med. Biol. 43(10):2677-83, 1998.

5) Feldkamp, LA, Davis, LC, and Kress, JW, J. Opt. Soc. Am. 1(6):612-9, 1984.

6) Hsieh, J, Molthen, RC, Dawson, CA, and Johnson, RH, these proceedings.

7) Davis, GR, Elliott, JC, and Anderson, P, In: X-ray Microscopy III, Michette, AG, Morrison, GR and Buckley, CJ (eds.), Springer, Berlin, 1992, pp.458-60.

8) Jennings, RJ, Med. Phys. 15(4):588-99, 1988.

9) Illerhaus, B, Goebbels, J, Riesemeier, H, et al., Proc. SPIE vol. 3149, pp101-6, 1997.

10) Davis, GR, Proc. SPIE vol. 3149, pp.213-21, 1997.